Materials Today Bio 16 (2022) 100400

Contents lists available at ScienceDirect

Materials Today Bio

journal homepage: www.journals.elsevier.com/materials-today-bio

Impact of aromatic residues on the intrinsic disorder and transitional behaviour of model IDPs

C. García-Arévalo [a], L. Quintanilla-Sierra [a], M. Santos [a], S. Ferrero [b], S. Acosta [a,1], J.C. Rodríguez-Cabello [a,*]

[a] GIR Bioforge, Universidad de Valladolid, CIBER-BBN, Paseo de Belén 9, 47011, Valladolid, Spain
[b] GIR MIOMeT, IU CINQUIMA/Química Inorgánica, Facultad de Ciencias, Universidad de Valladolid, 47011, Valladolid, Spain

ARTICLE INFO

Keywords:
Intrinsically disordered proteins
Elastin
Protein block co-polymers
Self-assembling materials

ABSTRACT

Understanding the interplay between order and disorder in intrinsically disorder proteins (IDPs), and its impact on the properties and features of materials manufactured from them, is a major challenge in the design of protein-based synthetic polymers intended for advanced functions. In this paper an elastin-like diblock co-recombinamer amphiphile (Phe-ELR) based on a hydrophobic block containing five phenylalanine (Phe) residues proximal to the carboxyl function of a glutamic acid (Glu) residue upon folding, and with Glu as the guest residue in the hydrophilic part, was engineered and its assembly behaviour compared with another amphiphilic ELR used as control. Phe-ELR was tailored in order to clarify the impact of the presence of aromatic residues in the amino acid sequence, which even in early studies by Urry's group already demonstrated a certain out-of-trend behaviour compared with other apolar amino acids, especially non-aromatic ones, on ELR behaviour. The combination of several experimental techniques indicates strong molecular interactions associated with the Phe residue, thus resulting in limited reversible character of the temperature-induced transitions during sequential thermal cycles, a lower than expected transition enthalpy, and clear differences in its supramolecular assembly with respect to the control ELR. A distinctive pre-aggregated state for the Phe-ELR under any condition of pH and temperature is found. Eventually, this state gives rise to Phe-core micelles or a solid jelly-like material, depending on the concentration, pH and presence of salts. In conclusion, it appears that the presence of aromatic residues and their ability to promote strong inter- and intramolecular interactions at any temperature and pH causes a complete modification of the order-disorder interplay present in other, non-aromatic ELRs. These molecular events have a profound impact on the physical properties of the resulting polymer when compared with other ELRs. This work helps to shed light on the limits that govern intrinsic disorder in ELRs beyond its inverse temperature transition.

1. Introduction

Unique combinations of common design motifs or molecular building blocks assembled in a precise manner have characterized the nano/microstructure of a wide variety of natural structural components over millions of years of evolution. As such, materials science usually attempts to mimic the features of these natural architectures in the development of synthetic functional materials [1].

One of the most ubiquitous mechanisms that nature practises is molecular self-assembly, which is the "*spontaneous association of molecules, through non covalent bonds and under equilibrium conditions, into stable, structurally well-defined aggregates and usually implies the presence of molecules consisting of two or more chemically distinct and frequently immiscible blocks that are covalently bound together*" [2].

Even though the above might suggest that a strict order is the key feature in life and materials sciences, some degree of disorder also plays an important role in nature, especially in the field of proteins, where intrinsically disordered domains are highly abundant [3]. Consequently,

* Corresponding author. Profesor José Carlos Rodríguez Cabello: BIOFORGE LAB, University of Valladolid. Campus Miguel Delibes. Edificio LUCIA. Paseo de Belén, 19. 47011 - Valladolid, Spain.
E-mail address: roca@bioforge.uva.es (J.C. Rodríguez-Cabello).
URL: http://www.bioforge.uva.es (J.C. Rodríguez-Cabello).
[1] The present affiliation of Dr. Sergio Acosta is Biohybrid & Medical Textiles (BioTex), AME - Institut für Angewandte Medizintechnik | Helmholtz-Institut, RWTH Aachen University, Forckenbeckstr. 55, 52074, Aachen (Germany).

https://doi.org/10.1016/j.mtbio.2022.100400
Received 17 June 2022; Received in revised form 10 August 2022; Accepted 11 August 2022
Available online 18 August 2022

the category of intrinsically disordered proteins (IDPs) has been introduced [4]. Some biological interactions require proteins to be fully or greatly disordered, adopting a "conformal selection" of the disordered domains in order to play a role in most fundamental biological processes [3]. Moreover, order and disorder are not exclusive, and highly ordered and well-defined structures sometimes arise from the disorder–order interplay, as happens during biomineralization [5] or with the proteins involved in nuclear membrane traffic [6]. One of the underlying ideas that support the functionality of most IDPs in biological systems is that they cannot establish sufficient inter-residue contacts to overcome the large decrease in conformational entropy resulting from their folding; however, their inherent flexibility allows them to adopt an ensemble of conformations in solution in order to fulfil their biological role. In light of the above, key aspects of these intrinsically disordered proteins must be elucidated and characterized in detail, thereby shedding some light on the limits that govern intrinsic disorder.

In an attempt to discern the underlying mechanism that governs this "order-disorder interplay", the self-assembly of block co-polymer amphiphiles has attracted considerable attention over many years given the wide variety of morphologies and applications that mimic those present in nature [2,7]. In this sense, the *de novo* design and recombinant synthesis of IDP-based polymers with controllable material properties, such as elastin and its derivatives [7,8], provides reproducible methods for the investigation of structural features with promising applications [9,10]. D. W. Urry pioneered studies into the molecular origins of chain disorder by identifying one of the most extensively studied IDPs based on the primary sequence of tropoelastin [7,11]. The low-complexity sequence and other structural premises that govern both its structure and functions led to the development of elastomeric biomaterials, which mimic the ability of native tissues to stretch under stress [12]. One of the most important families of IDPs are Elastin-Like Recombinamers (ELRs) that were available once recombinant expression was sufficiently well advanced to provide sufficient quantities of pure material in bacterial expression systems [13].

Glycine (G), valine (V), proline (P), and alanine (A) residues dominate (>80%) the overwhelmingly hydrophobic primary sequence responsible for the elastic properties of the protein. The high combined proline and glycine (PG) content, which enables the backbone to remain disordered even when aggregated, and the inability to bury all hydrophobic residues away from solvent, are the main drivers for an entropy-driven mechanism that governs the structural heterogeneity and contributes to the elasticity of elastin [11]. The conformational disorder of elastin and its derivatives is a constitutive feature of the structure and function of elastin and is based on its "*evolutionary simplicity*" and the high proline and glycine content [8,14].

IDPs and elastin itself share structural characteristics based on their flexibility in solution and conformational disorder that make them fully functional. However, while disordered sequences on IDPs typically combine low mean hydrophobicity and high net charge, elastin exhibits the opposite, namely an overwhelmingly hydrophobic primary sequence [15,16]. Until very recently, the fields of IDPs and elastin derivatives were studied independently. However, in view of their functional similarities, the mechanisms governing their common rules have begun to be studied jointly. These studies have been boosted by the ability to recombinantly produce homogeneous preparations of elastomeric derivatives in high quantities.

Most ELRs comprise repeat units of the pentapeptide (Val-Pro-Gly-**Xaa**-Gly)$_{\mathbf{n}}$ [13,17]. ELRs undergo an inverse temperature transition at a characteristic temperature (T_t), above which a phase separation from bulk water occurs. The hydrophobicity and mean polarity of ELRs are the parameters that affect T_t the most, such that an increase in hydrophobicity results in a decrease in T_t, and vice versa [18]. Similarly, the identity of **Xaa** and **n** are the main parameters controlling the phase behaviour as they determine the sensitivity of ELRs to pH, light, or ion concentration and other variables. Both these parameters influence the mean polarity of the ELR molecule and, as such, have been exploited to precisely manipulate T_t and, therefore, determine the final ELR assembly. For example, when pH-sensitive acidic or basic amino acids are placed at some of the **Xaa** positions, the T_t of these ELRs also becomes pH-dependent [19,20].

The recombinant synthesis of amphiphilic block co-polymers from different ELR-based motifs has led to designs with interesting morphologies on the nano-to microscale as a result of their self-assembly [21,22]. These include micelles [23–25], vesicles [26], fibers [27] and hydrogels [28], along with other complex structures such as biomorphic colporate particles [29], spherulite-like structures [30], tubular structures [31] or functionalized artificial organelles [32]. The main strategy underlying such behaviour rises from the relative hydrophilicity/hydrophobicity between blocks, which triggers selective self-assembly in the presence of different stimuli, with heat being the most widely used and common stimulus [21].

Despite being poorly represented in natural elastin, phenylalanine (Phe; F) and isoleucine (Ile; I) are typically introduced into the guest residue positions of ELR sequences to enhance overall hydrophobicity and lower T_t. In contrast, substitution of that position with less hydrophobic or charged residues, such as lysine (Lys; K) or glutamic acid (Glu; E), raises T_t, thus ensuring that it is significantly above the physiological temperature and precluding ELR coacervation (e.g., charged E in water has a $T_t > 65\ ^\circ C$) [21,33]. However, the studies by Urry et al. had already suggested that the incorporation of progressively more hydrophobic amino acids (such as Phe or Ile) into a Glu-containing elastin-based polypeptide did not necessarily result in a linear decrease in the transition temperature, according to the hydrophobicity scale based on hydrophobic folding [18,34]. In addition, Urry et al. [35] also demonstrated that, in some Phe-based elastin-like molecular systems, the tertiary structure dominates over the primary structure, thereby altering the typical hydration shells of the hydrophobic and polar moieties when sufficiently proximal. These authors also demonstrated that differences in the proximity of two hydrophobically disparate residues (such as F and E) resulted in different pK_a values, depending on their arrangement.

Although the almost complete lack of aromatic moieties in elastin suggests they are not essential for the biological elastic recoil function, inclusion of these blocks contributes to the development of novel protein-based biomaterials. Some pioneering studies describing the importance of aromatic interaction in protein aggregation, and more specifically the role of phenylalanine can be found in bibliography (see, for instance Refs. [36–39]). Indeed, very recent studies involving phenylalanine [40–45] clearly show the current interest in this amino acid. For instance, Mondal and Haldar have proposed [45] an out-of-equilibrium phenylalanine-based hydrogel for the development of advanced functional materials.

Herein we have engineered and characterized the assembly of a phenylalanine-based elastin-like diblock co-recombinamer (Phe-ELR) amphiphile as a function of pH, concentration and temperature. We have combined a polar hydrophilic ELR block (E-block) containing Glu as guest residue in one pentapeptide out of five with a hydrophobic block (F-block) including five Phe residues and one Glu residue per 30-mer (see Table 1).

The rationale behind this block design is that the presence of the guest residues E and F not only maximizes the hydrophilicity/hydrophobicity interplay in these residues between both blocks, but also within the same block. The architecture of our Phe-ELR has been selected in order to investigate Urry's previous observations [34,35] that assume an atypical behaviour of ELRs containing Glu residues when several Phe residues (five in Phe-ELR) are proximal to the carboxyl function. Phe-ELR has been characterized using several experimental techniques that provide key insights to quantify its structure for assessing intrinsic disorder and the impact of pH and concentration on the final assembly of the whole ELR.

The behaviour of our Phe-ELR has been compared with that of another di-block ELR (Ile-ELR) (Table 1) previously reported by our group [23,46–48] that will be used as the control ELR. Both ELRs share

Table 1
Sequence and molecular weights (MW) of the two ELRs under study, with glutamic, isoleucine and phenylalanine amino acids highlighted in colour. ***MALDI-TOF results**.

ELR	Sequence	MW (Theoretical)	MW (Experimental)*
Phe-ELR	MESLLP-[(VPGVG)$_2$(VPG**E**G)(VPGVG)$_2$]$_{10}$-(VGVPGVG**F**PG**E**G**F**PGVGVPGVG**F**PG**F**G**F**PG)$_8$-V	43387 Da	43115.3 ± 53 Da
Ile-ELR	MESLLP-[(VPGVG)$_2$(VPG**E**G)(VPGVG)$_2$]$_{10}$-(VG**I**PG)$_{60}$-V	46981 Da	46999.0 ± 20 Da

the same glutamic-based hydrophilic block (E-block), but Ile-ELR has isoleucine as a guest residue in the hydrophobic part (I-block) and is insensitive to pH. Moreover, both ELRs show its transition temperature in the same and convenient range. Glu and Phe residues in the Phe-ELR hydrophobic block maximize the difference between hydrophilicity and hydrophobicity by polarity; thus, the presence of interspaced Glu residue into this block attenuates the high hydrophobicity of Phe residues, and allows this hydrophobic block to have an effective mean polarity similar to that of the hydrophobic block of Ile ELR. For these two constructs, which have a similar MW, architectures, low complexity sequence domains and the presence of exactly the same proportion of structurally disruptive amino acids with the same Gly/Pro content (0.79), we will demonstrate a quite different behaviour with respect to the features that unite ELRs and IDPs.

2. Experimental section

2.1. Materials

The cloning and molecular biology for gene construction of the ELRs were performed by recursive directional ligation using standard genetic engineering methods, as reported previously [23,46,49].

ELR expression and purification were performed as follows. ELRs were expressed using a modified pET7 expression vector that was transformed into *E. coli* strain BLR (Phe-ELR) or BL21 (DE3) (Ile-ELR). The sequence of both the Phe-ELR amphiphile and Ile-ELR are shown in Table 1.

Liquid cultures of 20 mL E. *coli* harboring plasmids encoding ELRs were inoculated from frozen DMSO stocks in LB medium supplemented with glucose (1%) and 100 μg/ml ampicillin (Formedium). After 16 h of culture, each 20 ml aliquot was used to inoculate eight 1 L flasks containing 0.5 L of TB medium (Formedium) supplemented with 100 μg/ml ampicillin (Formedium). This TB medium is supplemented with glucose and alpha lactose for the auto induction of protein expression under the control of isopropylthiogalactoside (IPTG)-inducible promoters in *E. coli*. The flasks were then warmed at 37 °C in a shaker incubator at 250 rpm for 16 h. The cells were harvested by centrifugation at 5500×*g* for 15 min at 5 °C then resuspended in 500 ml of cold 20 mM Tris-based buffer. Cells were disrupted by sonication in an ultrasonic equipment (Misonix 750 W) at 1500 bar, on ice. DNA and cellular debris were precipitated by acidification with HCl 3.7% until pH 4. Samples were then centrifuged at 15,000×*g* and 5 °C. The supernatant containing the ELRs was purified using cycles of inverse transition cycling until a single band corresponding to the MW of each construct was observed in the SDS-PAGE gel. Thus, the supernatant was heated at 37 °C for 50 min to trigger phase separation of the ELRs. The precipitated ELRs were centrifuged at 8000×*g* at 40 °C and, after discarding the supernatant, they were cooled on ice overnight to re-dissolve the ELRs.

Some experimental details about the yield of the purified ELRs, and SDS-PAGE gels of the purified ELRs or the MALDI-TOF spectra (see Figure S1) are included in the Supporting Information.

2.2. Mass spectrometry

The MW of the ELRs was measured by matrix-assisted laser desorption/ionization time-of-flight mass spectrometry (MALDI-TOF) using a Bruker Autoflex instrument with ultrapure water to adsorb the sample into the matrix at 1 mg/ml. The values in Table 1 represent the mean value and standard deviation (SD) of three different measurements.

2.3. Acid-base titrations

The acid-base titrations were carried out as described previously by Urry et al. [50]. Briefly, 30 mg of each ELR were dissolved overnight in 1.5 ml of Milli-Q water in a 5 ml vessel. Each ELR solution was then adjusted to an initial pH value of around 2 using HCl or NaOH. The automatic T50 titrator (Mettler Toledo) was calibrated with standard pH solutions at pH 4, 7 and 9 and then programmed for the sequential addition of a 15 μl drop of NaOH 0.1 M every 45 min. The pH adjustment and all titration procedures were performed at 5 °C to prevent ELR folding as far as possible. Samples were maintained with constant magnetic stirring throughout the process. Titration curves were performed in triplicate and the results are given as the average value of the three measurements. Equivalence points reach a maximum value when calculating the first derivative of the titration curves. The midpoint is half of the equivalence point and the pK_a of each glutamic acid residue was determined using the Henderson–Hasselbalch approximation at the midpoint, where pH = pK_a.

2.4. Turbidimetric characterization

Turbidity experiments were conducted using a Varian Cary 100 UV–Vis spectrophotometer (Varian Inc., NC, USA) with a temperature-controlled cuvette holder. Optical density (O.D.) was assessed by the change in absorbance at 350 nm (Abs 350 nm) for 1 mg/ml ELR solutions as a function of temperature (ranging from 5.0 to 50.0 °C). Three sequential cycles of heating and cooling were programmed at 1 °C/min with a 120-s period for temperature stabilization. The absorbance values at 350 nm were plotted relative to the initial O.D. value.

2.5. Light scattering

Dynamic light scattering (DLS) was carried out to determine the hydrodynamic diameter (D_h) of the ELRs using a Zetasizer Nano ZSP (Malvern Instrument). ELR solutions at 1 mg/ml in water (at different pHs) or PBS were handled in a cold chamber until the beginning of the measurements. Three sequential heating/cooling cycles were applied to each sample (with temperature increases of 3 °C). Once the corresponding temperature had been reached, the sample was allowed to stabilize for 120 s prior to analysis. Three acquisitions were performed at

each temperature and the results are presented as the mean $D_h \pm$ standard deviation (SD) at the beginning and end of each cycle (5 and 50 °C, respectively). The polydispersity index (PDI) is shown in the same way for the three acquisitions.

2.6. Zeta potential measurements

Zeta potential measurements were carried out using a Zetasizer Nano ZSP (Malvern Instrument) at 25 μM (1.1 mg/ml) in water at different pHs. Three sequential heating/cooling cycles were applied to each sample (with temperature increases of 3 °C). Once the corresponding temperature had been reached, the sample was allowed to stabilize for 2 min prior to analysis. Each sample was measured at least ten times per acquisition and the data represent the mean and standard deviation (SD) of three different acquisitions at the beginning and end of each cycle (5 and 50 °C, respectively).

2.7. Cryo-transmission electron microscopy (Cryo-TEM) characterization

Lyophilized ELRs were dissolved at 1.1 mg/ml in pre-chilled water (at different pHs) or PBS and kept at 4 °C overnight, then the pH was accurately adjusted while maintaining the low temperature to prevent ELR folding as far as possible. The adjusted samples were subjected to three heating and cooling cycles up to 50 °C.

Four microliters of each sample were deposited on a freshly glow-discharged Cu 200 mesh grid (R 2/2 Holey Carbon Films; N1–C16nCu20-01; Quantifoil®, Germany) inside the chamber of a Vitrobot Mark III (FEI Company, USA), at a temperature of 50 °C and relative humidity close to saturation (90%). After incubation for 30 s the excess liquid was removed by blotting (blot time: 3 s; number of blots: 1; drain time: zero; blot offset: 2 mm). After the blotting step, the grid was plunged into the liquid ethane bath, previously cooled with liquid nitrogen at approximately −180 °C. Once the specimen had frozen, the vitrified grids were removed from the plunger and stored under liquid nitrogen.

Vitrified grids were cryo-transferred (−174 °C) in a 626 DH cryo transfer holder (Gatan Inc., USA) and analyzed using a JEM-2200FS/CR transmission electron microscope (JEOL Europe, Croissy-sur-Seine, France).

No-tilted zero-loss two-dimensional (2D) images were recorded under low-dose conditions, with a total dose of around 20–30 electrons $Å^{-2}$ per exposure, at defocus values ranging from 2.5 to 5.0 μm. The in-column Omega energy filter of the microscope helps to enhance the signal-to-noise ratio (SNR) by zero-loss filtering, using an energy selecting slit width of 20 eV centered at the zero-loss peak of the energy spectra. Digital images were recorded using a 4 K × 4 K (15 μm pixels) Ultrascan4000™ charge-coupled device (CCD) camera (Gatan Inc., USA) using DigitalMicrograph™ (Gatan Inc., USA) software, at a nominal magnification of 20,000 and 30,000 × resulting in a final sampling of 5.69 and 3.54 Å $pixel^{-1}$, respectively.

Self-assembled structures were analyzed with *ImageJ* software and their sizes (mean ± standard deviation) calculated over more than 250 nanoparticles.

2.8. Circular dichroism (CD)

The secondary structure of the ELRs was measured by CD spectroscopy in water and PBS pH 7.4 using a Jasco J815 apparatus with sample temperature controller (Tokyo, Japan), by scanning 0.1 (Ile-ELR) and 0.3 mg/ml (Phe-ELR) solutions of the ELRs in the far UV. The spectra were acquired at 5 °C and 50 °C in a cell (path length: 0.1 cm) at a speed of 50 nm/min. The resulting spectra is the average of four scans. Secondary structure percentages were quantified from the CD data (range 190–250) using BeStSel [51,52] (Beta Structure Selection) web server in the 200–250 nm range (when the dynode voltage was below 500 V).

2.9. Nuclear magnetic resonance (NMR)

NMR spectra were recorded using 500 MHz Agilent DD2 instruments equipped with a cold probe in the Laboratory of Instrumental Techniques (LTI) Research Facilities, University of Valladolid. ^{1}H and ^{13}C chemical shifts (δ) are reported in parts per million (ppm) and are referenced to tetramethylsilane (TMS), using the residual solvent peak as an internal reference. Standard abbreviations are used to indicate multiplicity: s, singlet; d, doublet; t, triplet; m, multiplet and br, broad signal. The NMR samples at different pHs (25 mg/ml) were dissolved in 650 μl of D_2O for internal lock and then transferred into a 5 mm NMR tube. In order to obtain a quantitative ^{1}H NMR spectrum the acquisition parameters were: 10 s relaxation delay between transients, 45° pulse width, spectral width of 8012 Hz, a total of 16 transients and 2.044 s acquisition time. ^{1}H and ^{13}C peak assignments were performed using 2D NMR methods. Homonuclear ^{1}H–^{1}H 2D experiments total correlation spectroscopy (zTOCSY) and nuclear Overhauser effect spectroscopy (NOESY) with a zero-quantum filter were used for artifact suppression [53]. zTOCSY experiments were acquired in the phase-sensitive mode using the WET pulse sequence in order to suppress the residual water signal resonance. A total of four transients for each of the 128 t1 increments were recorded, using a spectral width of 4960 Hz for both dimensions, with a mixing time for the DIPSI2 spin lock of 100 ms and an acquisition time of 150 ms. The data were apodized with Gaussian window in both dimensions. NOESY experiments were acquired using the WET pulse sequence to suppress the residual water signal resonance. A total of eight transients for each of the 128 t1 increments were recorded, using a spectral width of 5186 Hz for both dimensions, with a mixing time of 500 ms and an acquisition time of 300 ms. The data were apodized with Gaussian window in both dimensions. Carbon signals were detected indirectly using ^{1}H–^{13}C HSQC experiments. Gradient heteronuclear single quantum correlation (HSQC) spectra were acquired with inverse detection and carbon decoupling during acquisition in the phase-sensitive mode, with WET solvent suppression. A total of eight transients for each of the 128 t1 increments were recorded, using spectral widths of 8012 Hz in the F2 dimension and 25,133 Hz in the F1 dimension. A nominal value of 146 Hz was used for the one-bond coupling constant J_{CH}. The data were apodized with Gaussian function windows in both dimensions. Different temperatures from 5 to 50 °C were employed during the NMR studies. All spectra were manipulated and processed using Mestrelab Research software (MNova 12.0) and VnmrJ4.2 software (Agilent).

DOSY spectra of Phe ELR at 5 °C performed at 2.5 and 7–10 pHs were conducted on 500 MHz AgilentDD2 spectrometer using the Oneshot45 sequence (unbalanced bipolar pair gradient) [54,55]. The diffusion–encoding/decoding gradient strengths ranging from 6 to 50 Gcm^{-1} employing 20 gradient levels, 8 transients, a relaxation delay of 1.5 s, and the imbalance factor, α, of 0.2 were used. The diffusion period, Δ, was 700 ms with a length of the gradient pulses, δ, of 2.5 ms. The resulting DOSY spectra were processed using VnmrJ4.2 software (Agilent).

2.10. Differential scanning calorimetry (DSC) and thermally modulated DSC (TMDSC)

DSC and TMDSC were performed using a Mettler Toledo 822e device with liquid-nitrogen cooler. Both temperature and enthalpy were calibrated using standard samples of indium, zinc and n-octane. Aqueous solutions of the two ELRs were prepared at different concentrations (from 50 to 200 mg/ml). In all cases, 20 μl of the solution was placed inside a standard 40 μl aluminium pan and sealed hermetically. The same volume of solvent was placed in the reference pan. Both types of samples were maintained at 5 °C for 5 min to stabilize the temperature before starting measurements inside the sample chamber. DSC experiments were performed at a heating rate of 1 or 5 °C/min from 5 to 50 °C.

TMDSC was performed using a sinusoidal temperature fluctuation superimposed on a heating ramp with constant rate. The conditions were:

heating ramp (ν) = 1 °C/min; amplitude (A) = 0.1 °C; and period (P) = 0.6 min. A 150 mg/mL aqueous solution of the ELRs was prepared and all experiments were repeated three times. Positive and negative enthalpies correspond to endothermic and exothermic processes, respectively.

3. Results and discussion

Phe-ELR has been studied in detail in this paper paying special attention on the interactions associated to the Glu and Phe residues in its hydrophobic block. As a control recombinamer, a model ELR, Ile-ELR, has been selected whose hydrophobic part includes isoleucine as a guest residue and keeping the same structure in the hydrophilic block for both ELRs (see Table 1). The presence of Glu and Phe residues –with noticeable dissimilar polarities-in the Phe-ELR hydrophobic block gives rise to an effective mean polarity similar to that of the hydrophobic block of Ile ELR.

A detailed characterization of the two di-block co-recombinamer ELRs considered was performed by combining several experimental techniques, namely titration, turbidimetry, dynamic light scattering (DLS) and zeta potential measurements, circular dicroism (CD), nuclear magnetic resonance (NMR), thermal techniques, and cryo-TEM.

3.1. Titrations

The impact of pH on the ELRs has been considered using acid-base titrations. Phe-ELR is an amphiphilic ELdcR comprising a well-known hydrophilic pH-responsive block with Glu as guest residue equally spaced every 25 amino acids, and repeated 10 times, and a hydrophobic block comprising a "*polytricosapeptide*" previously described by Urry [35] based on five neighbouring Phe residues that are located proximal to the Glu residues when considering the common β-spiral tertiary structure approach for ELRs.

Glu residues contain a γ-carboxylic function, which undergoes strong polarity changes between its protonated and deprotonated states as a consequence of changes in pH around its effective pK_a. As a result of the increase in pH, deprotonation results in an increase in the mean polarity of the polymer, which in turn causes a shift in T_t to higher temperatures and a decrease in transition enthalpy since the charged carboxylate moiety precludes hydrophobic hydration around the polymer [33]. Urry et al. demonstrated that the competition for hydration between polar and apolar side chains results in dramatic pK_a shifts of up to 3.8 units for the Glu residue. This effect was named *"apolar-polar repulsive free energy of hydration"* [50,56] and it takes place when the Glu residue is found in a fixed primary 30-mer structure progressively containing a high amount of Phe residues replacing less hydrophobic Val amino acids in a non-linear fashion.

In order to verify the pK_a shift between the two different Glu residues present in Phe-ELR, we performed an acid-base titration (Figure S2) of Phe-ELR and compared this titration curve with that for the control ELR containing the same pH-responsive Glu-based hydrophilic block but with a pH-insensitive Ile residue (Ile-ELR) in the hydrophobic part (Table 1). This Ile-based block maximizes the polarity difference between both elastin sequences, although to a lesser extent than Phe, thus allowing us to determine whether the presence of hydrophobic residues close to Glu affects their pK_a, but also whether the presence of an adjacent block has any influence.

Since pK_a values are temperature-dependent, the acid-base titrations in this study were carried out at 5 °C to prevent ELR transitions from hindering the protonation-deprotonation of Glu residues. As expected, Phe-ELR titration followed a double-sigmoid curve, corresponding to the three sequential stages in which the different Glu residues are progressively deprotonated. The Phe residue is about three times more hydrophobic (relative to Val) than Ile, according to the T_t-based hydrophobicity scale proposed by Urry [57]. For this reason, a shift in pK_a (of 1.3 units) was observed for the Glu residue in the proximity of the hydrophobic Phe residue (pK_a 4.63 after adding 0.78 ml of titrant at pH 9.25 at the equivalence point), with this shift being higher than that found for the Glu residue present in the hydrophilic block (pK_a 3.47). This latter showed the same pK_a value in both di-block co-recombinamers (Phe and Ile-ELRs), with a sharp transition after the addition of 0.71 mL of titrant to reach the equivalence point at pH 6.93, thus suggesting no mutual influence between carboxylic acid groups in adjacent polymer segments. Thus, these results agree with Urry's work, in which a shift in pK_a as large as 1.7 units was observed in different ELRs analogous to our hydrophobic block [34].

As such, the competition for hydration between the apolar (Phe residues) and polar groups (Glu residues) along with the aromatic interactions and aromatic-proton interactions within Phe-ELR cause a delay in the formation of COO^- until the pH is increased further. A detailed discussion of this point will be accomplished by NMR in subsection 3.5.

3.2. Turbidimetry

The phase behaviour of these two ELRs was initially studied by turbidity measurements. These measurements provide information about the self-assembling process of the ELRs by determining the intensity of sample turbidity above T_t. Turbidimetric characterization was performed at different pH values, depending on the corresponding pK_a value for the two glutamic acids determined in the titration measurements. Thus, the absorbance of 1 mg/ml ELR solutions at 350 nm at different pH values and in different solvents was monitored as a function of temperature (Fig. 1).

Aqueous solutions at the lowest pH (pH 2.5 mQ) indicated the presence of complex transitions for both ELRs, although these systems differed in terms of the magnitude of turbidity at the highest temperature (50 °C). Thus, Phe-ELR showed a delayed and partially reversible multistep transition after the first heating cycle that did not reach the initial absorbance values. However, subsequent heating-cooling cycles almost overlapped. Initial changes for Phe-ELR started at temperatures as low as 6 °C, where a conformational organization is observed; additional changes occurring from 23.5 °C and higher. A similar turbidimetric profile was seen for Phe-ELR at pH 4, although it lacked the transition at temperatures between 6 and 15 °C found at pH 2.5. For Ile-ELR at pH 2.5, the turbidity began to increase from 22.5 °C and, similar to Phe-ELR, showed a wide hysteresis cycle, although unlike Phe-ELR all curves overlapped. Hysteresis is a phenomenon already described for other ELRs with different compositions and usually indicates structural changes that correlate with an increase in the number of side-chain contacts and reduction in localized water, thereby counteracting the thermally driven process [58,59]. The maximum absorbances for Phe-ELR and Ile-ELR at pH 2.5 are around 0.8 and 2.7, respectively. The low value found for Phe-ELR suggests the formation of a stable colloidal dispersion under pH conditions above the highest pK_a. When aqueous solutions at pH 7 are considered, Phe-ELR did not show any noticeable transition, but Ile-ELR maintained both the transition –with a transition temperature about 30°C- and the hysteresis –although with a minimal intensity, below 0.03.

If the effect of salts is present, Phe- and Ile-ELRs in PBS at pH 7 again showed some hysteresis, although a completely reversible behaviour was observed for both ELRs. In addition, the absorbance intensity is substantially reduced, and both turbidimetric profiles differed in magnitude, with an intensity fivefold higher for Ile-ELR than for Phe-ELR (both being minimal and below 0.05). Therefore, a lesser extent of hysteresis and completely reversible transitions for Phe-ELR are observed with increasing pH.

3.3. Dynamic light scattering and zeta potential measurements

The scattered light intensity of the ELRs as a function of temperature resulted in different size distributions, depending on pH and solvent (Table 2). Additionally, the zeta potential was measured to confirm the net charge of each sample under several pH conditions.

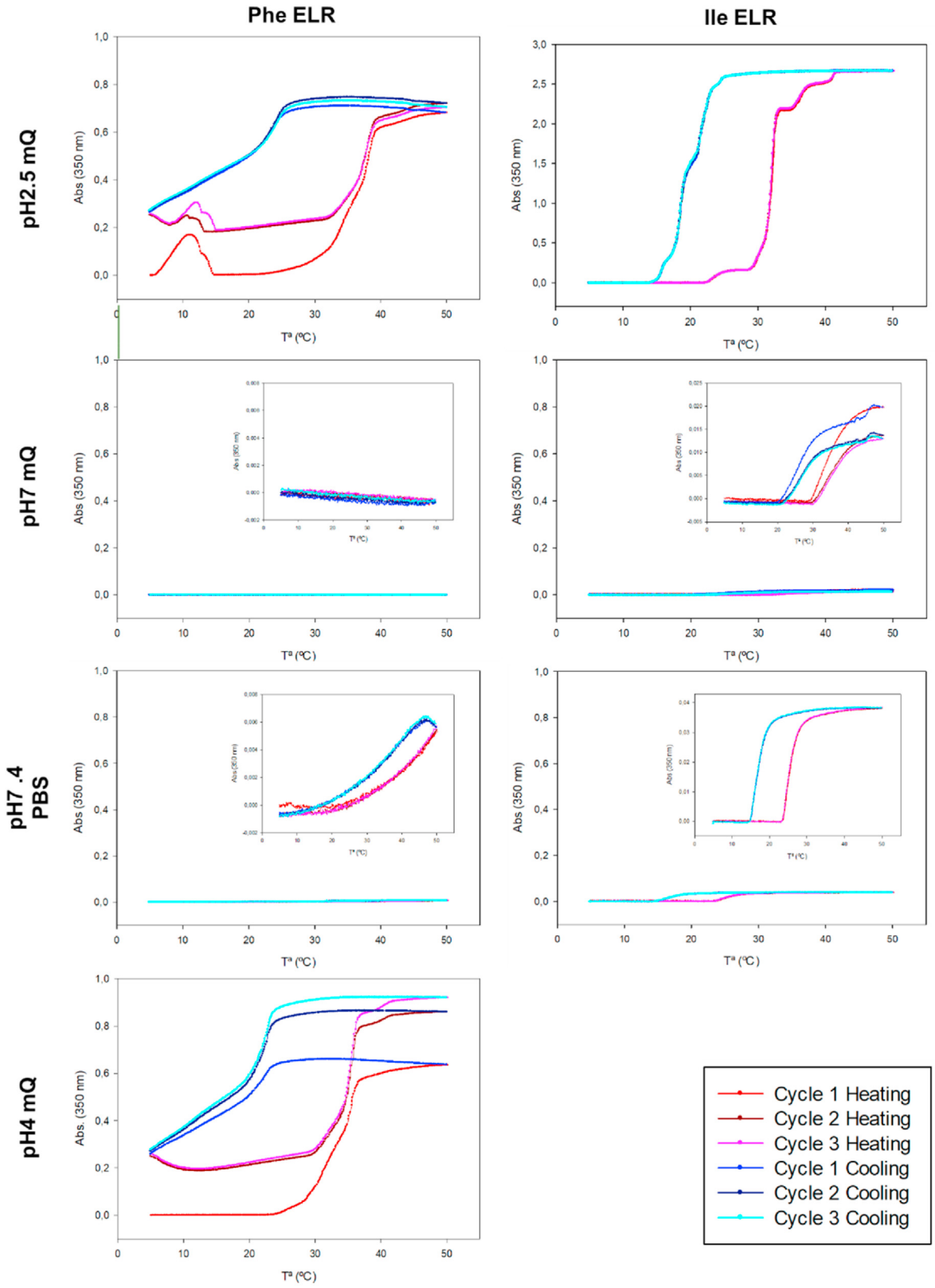

Fig. 1. Plots of normalized turbidity at 350 nm as a function of temperature; three consecutive heating and cooling cycles were applied. Some insets are included to appreciate in detail the change in optical density. PBS refers to phosphate saline buffer at pH 7.4 and mQ refers to Milli-Q water.

Table 2
Mean and standard deviation (SD) for the hydrodynamic diameter (D_h), polydispersity index (PDI) obtained by DLS and zeta potential of Phe and Ile ELRs after three consecutive heating-cooling cycles in different solvents and at different pH values.

	Phe-ELR pH2.5 mQ			Ile-ELR pH2.5 mQ		
T (°C) / (Cycle)	D_h (nm)	PDI	Zeta potential (mV)	D_h (nm)	PDI	Zeta potential (mV)
5 (ON)	**80.6 ± 8.73**	**0.27 ± 0.03**	+13.90 ± 8.06	1269.03 ± 1205.51	0.85 ± 0.20	+8.49 ± 6.49
50 (1st)	**88.71 ± 0.26**	**0.03 ± 0.00**	+1.62 ± 0.63	230.07 ± 1.19	0.18 ± 0.01	-0.01 ± 0.11
5 (1st)	**81.99 ± 3.12**	**0.09 ± 0.01**	+1.01 ± 0.75	38.56 ± 8.55	0.24 ± 0.09	+0.90 ± 0.69
50 (2nd)	**85.42 ± 1.03**	**0.03 ± 0.03**	-1.34 ± 0.42	228.57 ± 0.80	0.16 ± 0.01	-0.14 ± 0.14
5 (2nd)	**82.75 ± 3.13**	**0.12 ± 0.01**	-0.61 ± 0.21	28.55 ± 7.31	0.30 ±0.09	-0.41 ± 0.65
50 (3rd)	**85.14 ± 0.41**	**0.03 ± 0.01**	-0.05 ± 0.10	235.83 ± 1.84	0.19 ± 0.01	-3.04 ± 0.62
5 (3rd)	**84.16 ± 2.96**	**0.03 ± 0.02**	-1.09 ± 0.49	38.87 ± 8.67	0.28 ± 0.04	-0.39 ± 0.62
	Phe-ELR pH7 mQ			Ile-ELR pH7 mQ		
	D_h (nm)	PDI	Zeta potential (mV)	D_h (nm)	PDI	Zeta potential (mV)
5 (ON)	11.8 ± 3.53	0.63 ± 0.04	-17.20 ± 3.25	9.49 ± 0.08	0.26 ± 0.00	-0.99 ± 1.08
50 (1st)	2031.00 ± 909.35	0.90 ± 0.12	-13.40 ± 2.69	**148.00 ± 4.76**	**0.37 ± 0.07**	-30.73 ± 0.35
5 (1st)	**54.59 ± 36.17**	0.36 ± 0.06	-16.80 ± 1.21	8.64 ± 0.25	0.23 ± 0.01	-25.10 ± 2.23
50 (2nd)	1860.37 ± 981.54	0.87 ± 0.23	-17.60 ± 0.20	**130.43 ± 9.15**	**0.46 ± 0.09**	-30.87 ± 0.31
5 (2nd)	**29.41 ± 25.56**	0.56 ± 0.24	-19.20 ± 0.92	8.33 ± 0.10	0.20 ± 0.01	-22.77 ± 4.22
50 (3rd)	2771.67 ± 1329. 57	0.93 ± 0.12	-17.90 ± 0.26	**131.13 ± 8.31**	**0.41 ± 0.10**	-30.53 ± 0.32
5 (3rd)	**53.14 ± 17.46**	0.32 ± 0.02	-17.33 ± 0.21	8.64 ± 0.25	0.22 ± 0.01	-17.57 ± 3.88
	Phe-ELR pH7.4 PBS			Ile-ELR pH7.4 PBS		
	D_h (nm)	PDI	Zeta potential (mV)	D_h (nm)	PDI	Zeta potential (mV)
5 (ON)	21.85 ± 2.41	0.40 ± 0.01	n.d.	13.40 ± 0.63	0.25 ± 0.05	n.d.
50 (1st)	**27.49 ± 0.07**	**0.08 ± 0.00**	n.d.	**41.22 ± 0.31**	**0.01 ± 0.00**	n.d.
5 (1st)	21.55 ± 0.78	0.43 ± 0.01	n.d.	13.04 ± 0.50	0.23 ± 0.04	n.d.
50 (2nd)	**28.45 ± 0.17**	**0.12 ± 0.00**	n.d.	**41.53 ± 0.50**	**0.01 ± 0.00**	n.d.
5 (2nd)	25.19 ± 0.64	0.51 ± 0.02	n.d.	14.62 ± 0.79	0.31 ± 0.04	n.d.
50 (3rd)	**29.17 ± 0.24**	**0.14 ± 0.01**	n.d.	**41.50 ± 0.40**	**0.01 ± 0.00**	n.d.
5 (3rd)	26.21 ± 2.43	0.50 ± 0.03	n.d.	14.80 ± 0.23	0.34 ± 0.01	n.d.
	Phe-ELR pH4 mQ			Notes/ Abbreviations		
	D_h (nm)	PDI	Zeta potential (mV)	-**Bold numbers** correspond to monomodal populations (Intensity 100%).		
5 (ON)	**46.88 ± 0.47**	**0.05 ± 0.02**	+0.22 ± 0.14	-Un-bold numbers correspond to the mean D_h for a multimodal distribution in which a major peak with an intensity ≥85% has a size that approximates to the mean D_h.		
50 (1st)	**83.22 ± 1.04**	**0.04 ± 0.00**	-22.4 ± 0.61			
5 (1st)	**88.51 ± 3.92**	**0.10 ± 0.02**	-14.43 ± 1.36			
50 (2nd)	**90.86 ± 1.52**	**0.03 ± 0.02**	-31.77 ± 0.40			
5 (2nd)	**91.03 ± 4.32**	**0.11 ± 0.01**	-16.63 ± 0.40	-Grey values are not significant according to PDI values.		
50 (3rd)	**91.45 ± 0.75**	**0.03 ± 0.02**	-29.07 ± 0.81	-ON: incubation overnight		
5 (3rd)	**90.97 ± 2.51**	**0.11 ± 0.04**	-16.27 ± 0.40			

When the temperature is initially stabilized at 5 °C before starting the heating-cooling cycles, Phe-ELR at pH 2.5 in Milli-Q water showed a broad yet monodisperse band with a mean hydrodynamic diameter (D_h) of 80.6 ± 8.73 nm and a polydispersity index (PDI) of 0.27 ± 0.03. This band progressively narrowed (lowering polydispersity), while D_h remains around 80–90 nm over successive cooling-heating cycles. Under these conditions, the zeta potential remained close to zero, as expected (Table 2). At pH 4 in water, Phe-ELR showed a similar trend to the previous condition, although the size of the nanoparticles before heating the sample for the first time was around half that found at pH 2.5 (D_h = 46.88 ± 0.47 nm; PDI = 0.05 ± 0.02). Surprisingly, after the first heating cycle, at this pH Phe-ELR reached a nanoparticle size similar to that achieved at pH 2.5 (D_h = 83.22 ± 1.04 nm; PDI = 0.04 ± 0.00), with this value subsequently remaining stable and again about 80–90 nm. At pH 4, only the Glu residues of the hydrophilic block should remain charged, while those present in the hydrophobic block should be protonated. In this case, the zeta potential almost doubled in value when the temperature increased during the second and third cycles. Taking into account an initial and partially hindered conformational organization before temperature cycles, the major reason for this effect is likely different equilibrium structures accessible via temperature cycles which additionally allow formerly "frozen" hindered structures induced by the Phe-Interactions are resolved. A partial delocalisation of the negative charge might be also suggested. This large negative value of the zeta potential is generally considered to be dominant over van der Waals forces, thus meaning that agglomeration is suppressed due to electrostatic repulsion between individual particles [60]. In accordance with the turbidimetric variations shown previously, these D_h and zeta potential results suggest that Phe-ELR is present in a pre-aggregated state at this concentration at pH 2.5 and 4.

Multimodal distributions –with quite elevated PDI values-were recorded for Phe-ELR at pH 7 in water. It should be noted that the D_h value must be considered carefully in these cases. In addition, the zeta potential shows no significant change as the temperature is increased from 5 to 50 °C in the sequential cycles. The presence of deprotonated Glu residues in both the hydrophobic and hydrophilic blocks should prevent the formation of any assembly in water at any temperature. At pH 7.4 in PBS, the presence of salts masks all the charged residues, thus

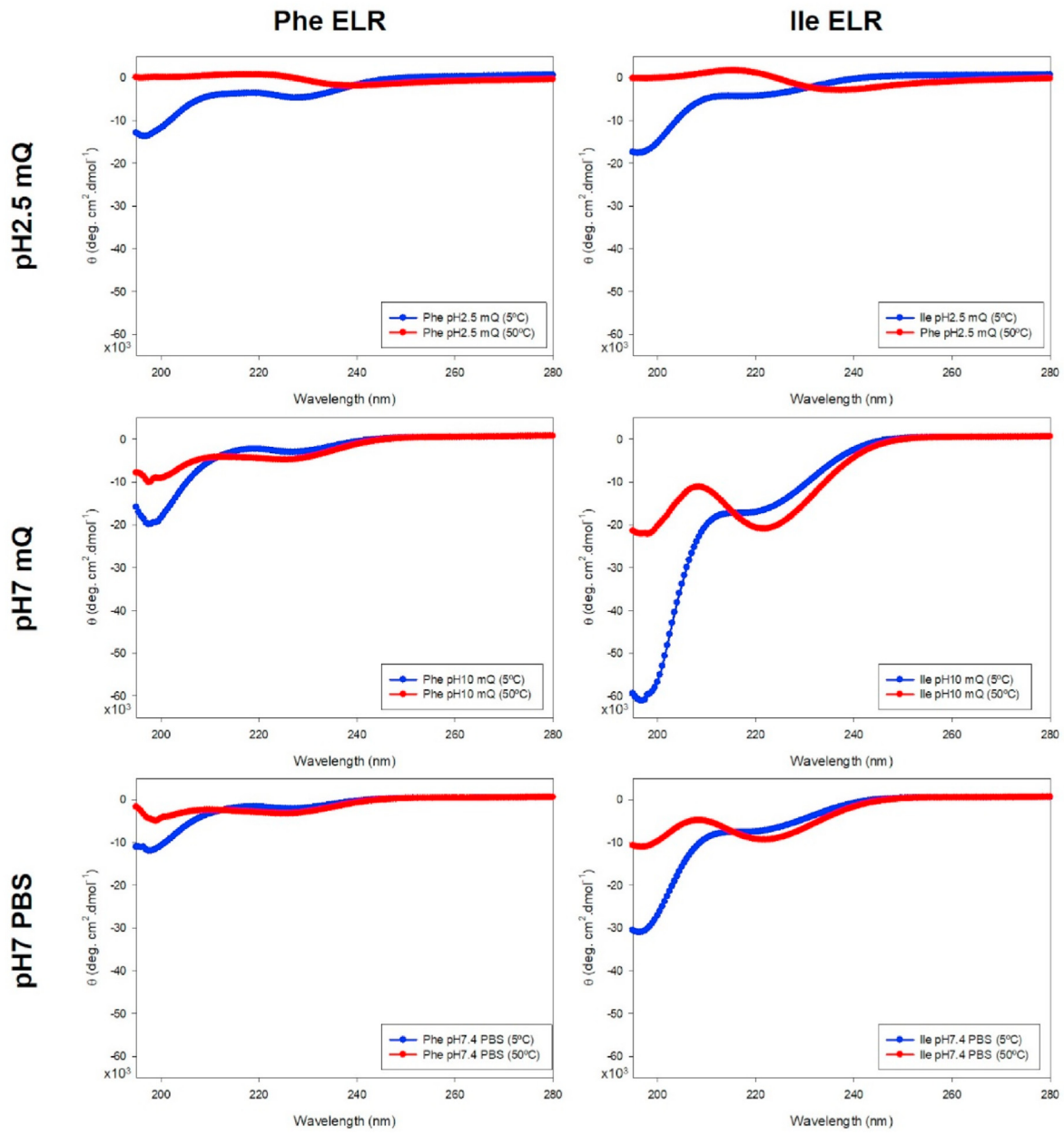

Fig. 2. CD spectra of Phe and Ile ELRs at a concentration of 0.3 and 0.1 mg/ml, respectively, at different pH values (2.5, 7 and 7.4), in different solvents (Milli-Q water and PBS) and at different temperatures (5 °C: blue lines, and 50 °C: red lines).

allowing the formation of highly monodisperse nanoparticles at the highest temperature (50 °C) with a size three times smaller than that obtained at pH 2.5 (D_h = 29.17 ± 0.24 nm; PDI = 0.14 ± 0.01 at 50 °C after the third heating cycle).

The thermally driven assembly of Ile-ELR, as monitored by DLS, showed a different self-organization. Thus, at 50 °C and at the lowest pH, Ile-ELR showed a monodisperse particle distribution. After the first temperature cycle, the D_h varied between 30 and 40 nm and around 230 nm for temperatures of 5 and 50 °C, respectively, thus demonstrating the reversibility of this transition. These sizes are 2.5-fold higher than those found for Phe-ELR at the same pH (where size remains stable at around 80–90 nm). These differences may be related to the sequential transition of the two blocks present in Ile-ELR (18–20 °C for Ile block and 28–30 °C for the Glu block, according to the literature [47] and our results), a transition that is lacking (from a size viewpoint) in Phe-ELR ELR (see Figure S3 in Supporting Information). In addition to the differences during ELR packing, some other reasons may be suggested to explain this result, such as rather different interaction energies due to different side chains, and even Phe vs. Ile distribution.

At pH 7, Ile-ELR formed monodisperse and reversible nanoparticles in both water and PBS at temperatures above ~20 °C, as reported previously [23,46]. The nanoparticles in water had a mean hydrodynamic diameter higher than that in PBS and a higher polydispersity (D_h = 131.13 ± 8.31 nm; PDI = 0.41 ± 0.10 versus D_h = 41.50 ± 0.40 nm; PDI = 0.01 ± 0.00 at 50 °C after the third heating cycle). At 50 °C in water a high negative zeta potential is found and this net charge may also be responsible for the higher sizes in water than in PBS since the masking effect of salts is lost.

The myriad of sizes and assemblies found in our DLS measurements fit into the different micellar states described by W. Hassouneh et al. [61], where a diagram of states of amphiphilic ELR di-blocks that display temperature-triggered self-assembly corresponds to different spherical "*weak*" or "*strong*" micellar states, depending on the core density and coronal stretching. The polarity changes with pH in the pH-responsive

blocks that comprise the ELRs under study are responsible for modifying the free-energy contributions in the core, corona, and core-corona interface. This fact, along with the natural propensity of these polypeptides to form secondary structures as they undergo their phase transition, produces a change in the rigidity of the chain for both blocks with increasing temperature [62,63].

3.4. Circular dichroism

CD spectroscopy was used to monitor changes in the conformation of the ELRs in both water (pH 2.5 and pH 7) and PBS (pH 7.4), and at two different temperatures (5 °C and 50 °C) (Fig. 2).

All conditions studied exhibited two major structural characteristics of the "*natively unfolded*" proteins [64,65]: at 5 °C, a negative peak near 200 nm, and a less intense, negative shoulder centered at around 220 nm. All θ_{200} values decreased in magnitude upon increasing the temperature, a phenomenon already described for other ELRs [46,66]. Differences in θ_{200} peak intensities between Phe- and Ile-ELRs were remarkable at low temperature, as was the significant decrease (almost complete disappearance) when the temperature was increased to 50 °C in the two most extreme pH conditions. This decrease in CD signals may be associated with some increase of a specific conformation (for instance, relaxed antiparallel beta sheet increases at 50 °C for both ELRs), or even a greater tendency to aggregate may not be ruled out.

CD data were used to quantitatively estimate the secondary structure percentage using the BeStSel algorithm [51,67] (Table S1 and Figure S4). In most cases, β-strands were the second most frequent conformation after "*other structures*". The complete absence of parallel β-sheets in Phe-ELR under any condition was noticeable, and we suggest that the presence of Phe residues is responsible for this relevant feature. Given the minor differences found over the wide range of pH values, the CD analysis of Phe-ELR at pH 4 did not seem relevant. Moreover, although the differences in solvent polarity and ionic strength affected the structural distribution of antiparallel structures in both ELRs, a greater amount of relaxed antiparallel structures was observed for Phe-ELR at both temperatures (5 and 50 °C).

Following the θ_{200} and θ_{222} criteria proposed by Uversky et al. [64], "*signs of residual secondary structure*" indicate small regions with a stable secondary structure or a dynamic ensemble of structures. Therefore, the CD spectra confirm that the presence of Phe and Glu in the hydrophobic block conditions the native folding of Phe-ELR, thus giving rise to a different folding from that of Ile-ELR even at low temperatures.

Moreover, the BeStSel algorithm predicts "*other structures*" with percentages of around 45–60%, which makes a reliable interpretation of this category difficult since it includes 3,10 –helix, π-helix, β-bridge, bend, loop/irregular and invisible regions of the structure. For this reason, NMR structural analysis was performed to probe the structure and dynamics at a residue level instead of at a global level like CD.

3.5. Nuclear magnetic resonance

The ^{1}H NMR spectra of Ile-ELR were in good agreement with theoretical predictions for their polymeric structure and the dynamics described above. The spectra obtained at pH 7 showed the expected signals and integrals, such as those for the methyl groups of Ile at 0.8 and 1.2 ppm, which were present at 5 °C but absent at 50 °C (Figure S5B and D). Similarly, the ^{1}H NMR spectrum of Ile-ELR at pH 2.5 showed no significant differences with respect to the spectrum at basic pH and 5 °C, although it contained a signal at 2.1 ppm corresponding to the methylene groups of Glu in its protonated form. This signal was shifted from the broad signal at around 1.9 ppm (which usually overlaps the methylene of glutamic acid in its deprotonated form), and remained visible after increasing temperature to 50 °C, and a drastic broadening of most signals was also observed (Figure S5A and C). The absence of signals belonging to the I-block at high temperatures, and the presence of signals from the hydrophilic block only, agrees with the formation of nanoparticles with an external shell of the E-block and an I-block-based core, but with an apparent stronger coupling at lower pH values. This finding agrees with previous studies [61], which demonstrated a nanoparticle assembly with the hydrophobic block at the core of the resulting particles above T_t.

The ^{1}H NMR spectra recorded for Phe-ELR at pH 7 and 5 °C also agreed with the theoretical predictions for Phe-ELR chains (Figure S6G).

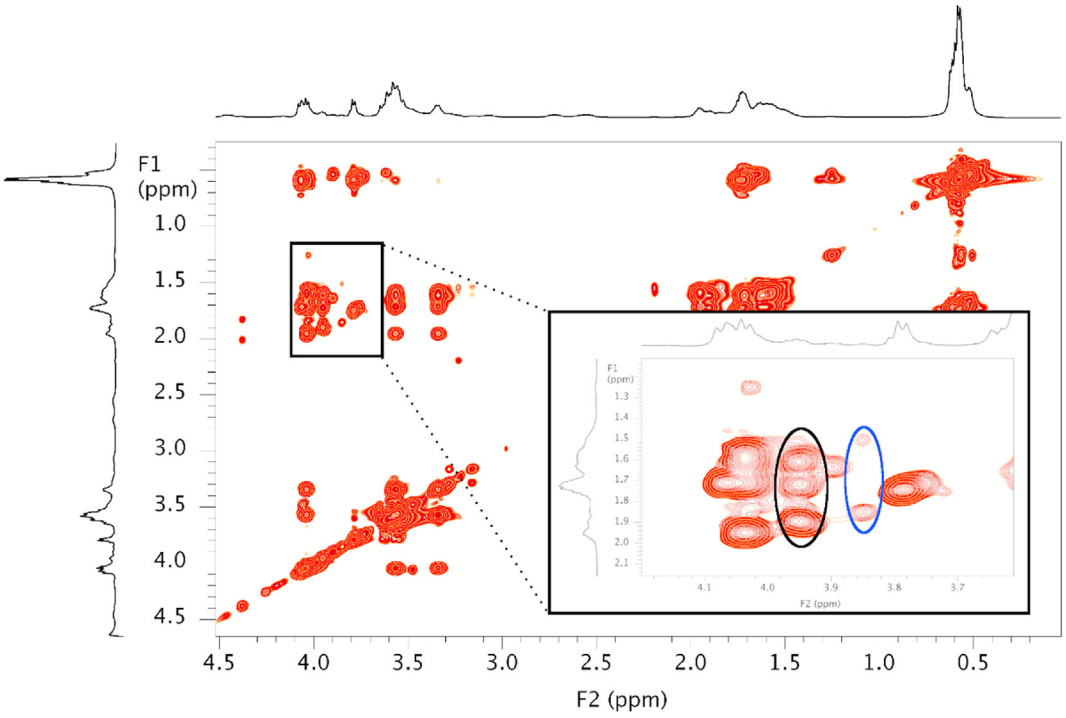

Fig. 3. TOCSY of Phe-ELR at pH 10 and 5 °C.

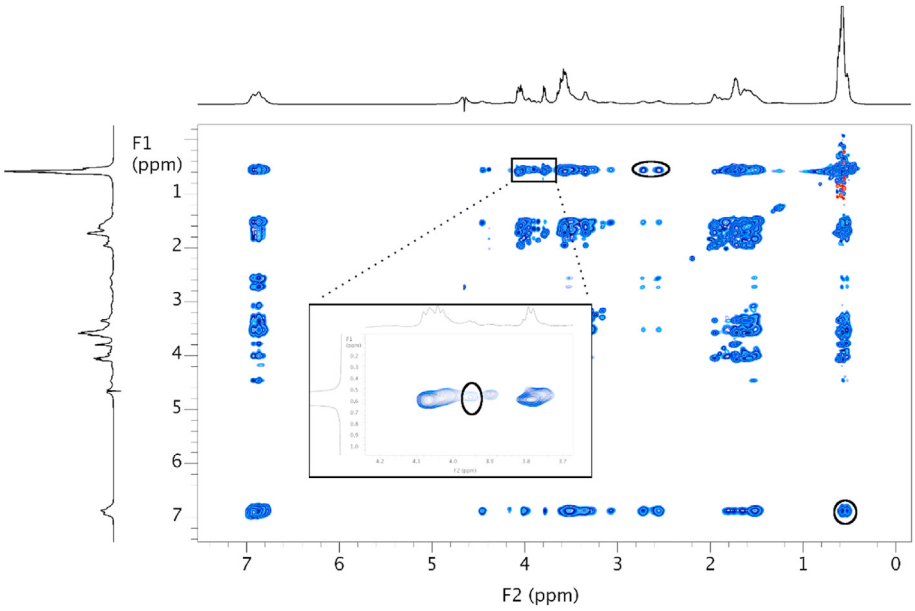

Fig. 4. NOESY of Phe-ELR at pH 10 and 5 °C.

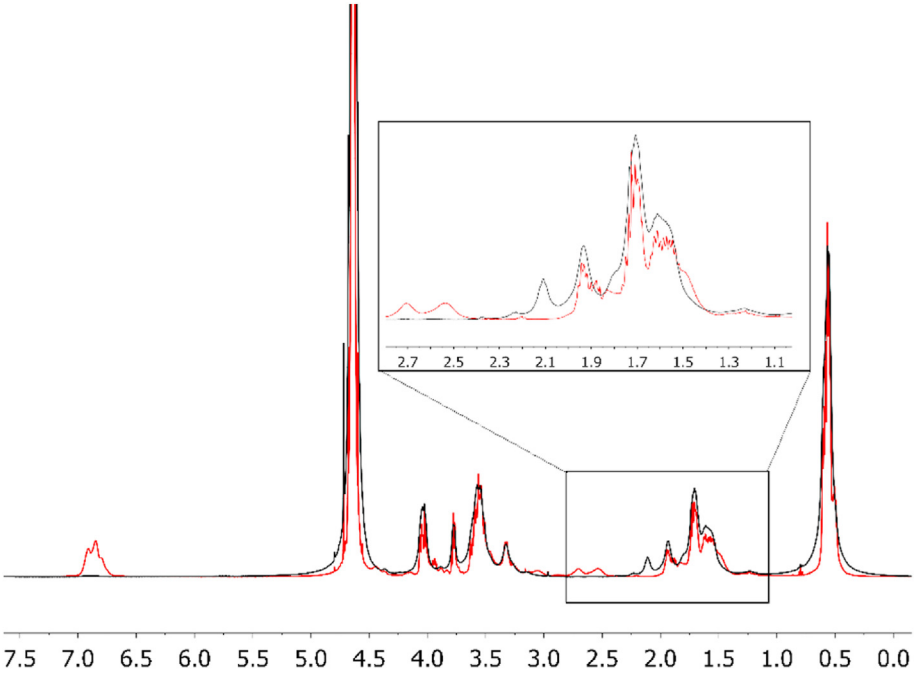

Fig. 5. Superimposed ^{1}H NMR spectra of Phe-ELR at pH 2.5 (black line) and pH 7 (red line) at 5 °C.

Under these conditions, the ^{1}H NMR signals were in agreement with the polymeric structure established, with the carboxylic groups of Glu in their deprotonated form, with the signals for the phenyl groups of Phe appearing at 6.80–6.70 ppm and the methylene of the benzylic groups at 2.71 and 2.53 ppm. In addition, the proton from the tertiary carbon of Glu appears at 3.95 ppm and one of the methylene groups of Glu is included in the broad signal at around 1.89 ppm. The integration of the aforementioned signals agreed with the theoretical predictions for a construct comprising "non-aggregated" Phe-ELR chains. Upon increasing the temperature to 50 °C, the ^{1}H NMR spectrum in the pH range 7–10 did not show great differences in either the chemical shifts of the signals or their respective integrals, which is consistent with the lack of an apparent transition for Phe-ELR detected using the previous techniques at this basic pH (Figure S6H). Nevertheless, as the temperature increased, the ^{1}H NMR signals for Phe-ELR become sharper and better defined, thus indicating a higher mobility for the polymer chains. It should be noted that the signals belonging to the phenyl and methyl groups of Phe were especially broad at low temperatures, probably due to phenyl-phenyl interactions in an ordered structure, and their narrowing as the temperature increased was especially noticeable.

A comprehensive TOCSY analysis of Phe-ELR at pH 7 and low temperatures showed the presence of two different methylene groups for the two different Glu residues: one from the polar block and the other from the Phe block. The first of these, which is in a polar environment, shows two chemical shifts for methylenes at 1.85 and 1.50 ppm (Fig. 3, TOCSY zoom, blue ellipse). In contrast, the Glu from the hydrophobic block

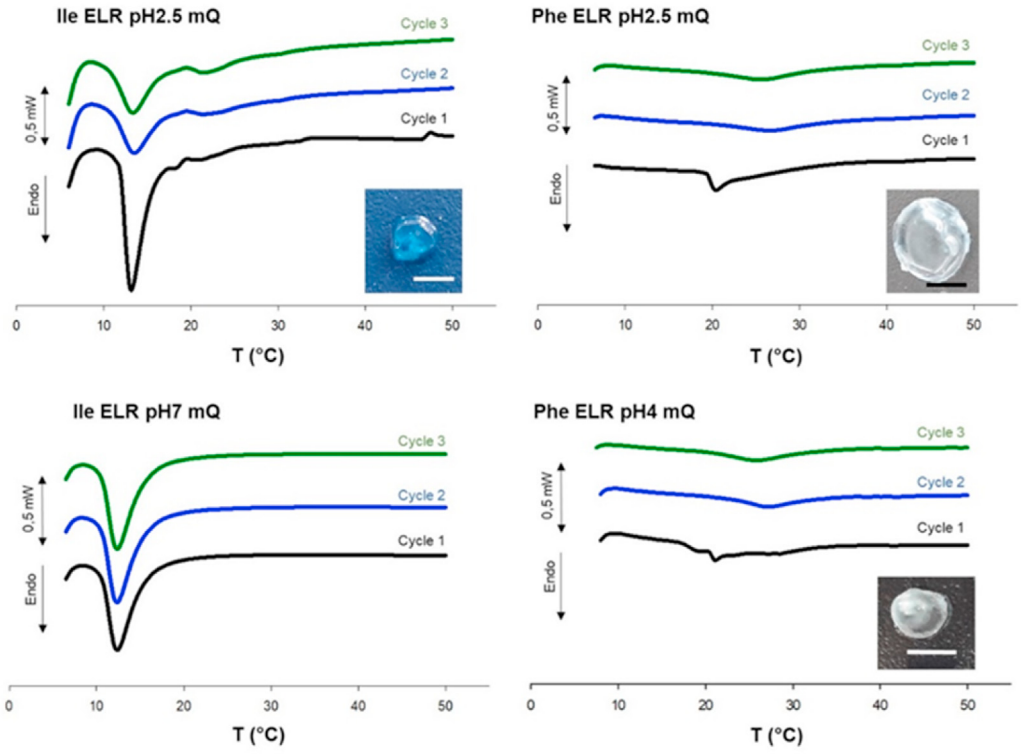

Fig. 6. DSC thermograms showing three subsequent cycles for 150 mg/ml aqueous solutions of Phe- and Ile-ELRs at a heating rate of 5 °C/min. The inserts show the hydrogels formed (if any) after the 3 cycles (scale bar: 0.3 cm).

shows a methylene at 1.89 ppm, with the protons from the other methylene groups, which are diastereotopic, appearing as two different signals at 1.72 and 1.60 ppm (Fig. 3 TOCSY zoom, black ellipse). The presence of diastereotopic protons at the methylene groups indicates a different chemical environment, which means they are differently accessible for the magnetic field and therefore exhibit different chemical shifts. This behaviour suggests a spatial organization. In this sense, it is worth noting that both the methylenes from benzylic groups and those from Glu are diastereotopic, and are probably in an ordered arrangement.

The NOESY spectrum for this molecule showed a proximity between the proton from the tertiary carbon of Glu and methyl groups from Val (Fig. 4, NOESY and zoom, black box). No other NOE signal was identified for the other methylene groups from the Glu of the hydrophobic block, which could agree with an arrangement of these groups away from the order of the rest of the Phe-based block.

Similarly, the presence of a NOE signal between both phenyl and benzyl groups and the methyl groups from Val (Fig. 4-NOESY, black circles) indicates proximity between those groups and, once again, suggests an ordered structure, in this case with proximity between the Phe and Val residues. Indeed, the NOE spectrum suggests that Phe groups are spatially located close to the Val groups and these Val groups are close to the Glu groups. This suggests a pre-ordered structure for the hydrophobic block even at low temperatures and high basic pH irrespective of the hydrophilic block fused to the hydrophobic one.

Surprisingly, the ^{1}H NMR spectrum for Phe-ELR at pH 2.5 and 5 °C showed the absence of signals for the Phe block at low temperature (Figure S6E), especially the loss of both signals for phenyl groups at 6.80–6.70 ppm and the absence of the methylene for the benzylic groups of Phe at 2.71–2.53 ppm. Moreover, integration of the ^{1}H NMR signals under these conditions was in perfect agreement with the exclusive presence of the E-based hydrophilic block. Indeed, a comparison of the integrals of the signals for the methylene groups from Glu in Phe-ELR at both pH values (2.5 and 7–10) showed a decrease of about 16 protons as a result of the disappearance of the signal for the methylene groups from the Glu in the hydrophobic block. In other words, the signals at 1.75–2.05 ppm, which integrate for 115 protons at pH 7 and 5 °C,

Table 3
Temperature transition (T_t) and transition enthalpy (ΔH) for three subsequent cycles in DSC thermograms for 150 mg/ml aqueous solutions of Phe- and Ile-ELRs at a heating rate of 5 °C/min.

Phe-ELR	pH2.5 mQ	pH4 mQ	pH7 mQ	pH7.4 PBS	Ile-ELR	pH2.5 mQ	pH7 mQ	pH7.4 PBS
	T_t: °C ΔH: J/g					T_t: °C ΔH: J/g		
Cycle 1	20.42 -6.21	20.05 -3.77	-	-	Cycle 1	12.23 -22.50	11.49 -8.65	10.98 -8.63
Cycle 2	26.67 -6.25	24.39 -6.47	-	-	Cycle 2	12.44 -18.33	11.52 -8.74	11.05 -8.87
Cycle 3	25.59 -6.09	24.65 -7.20	-	-	Cycle 3	11.91 -21.18	11.56 -9.14	11.00 -8.84

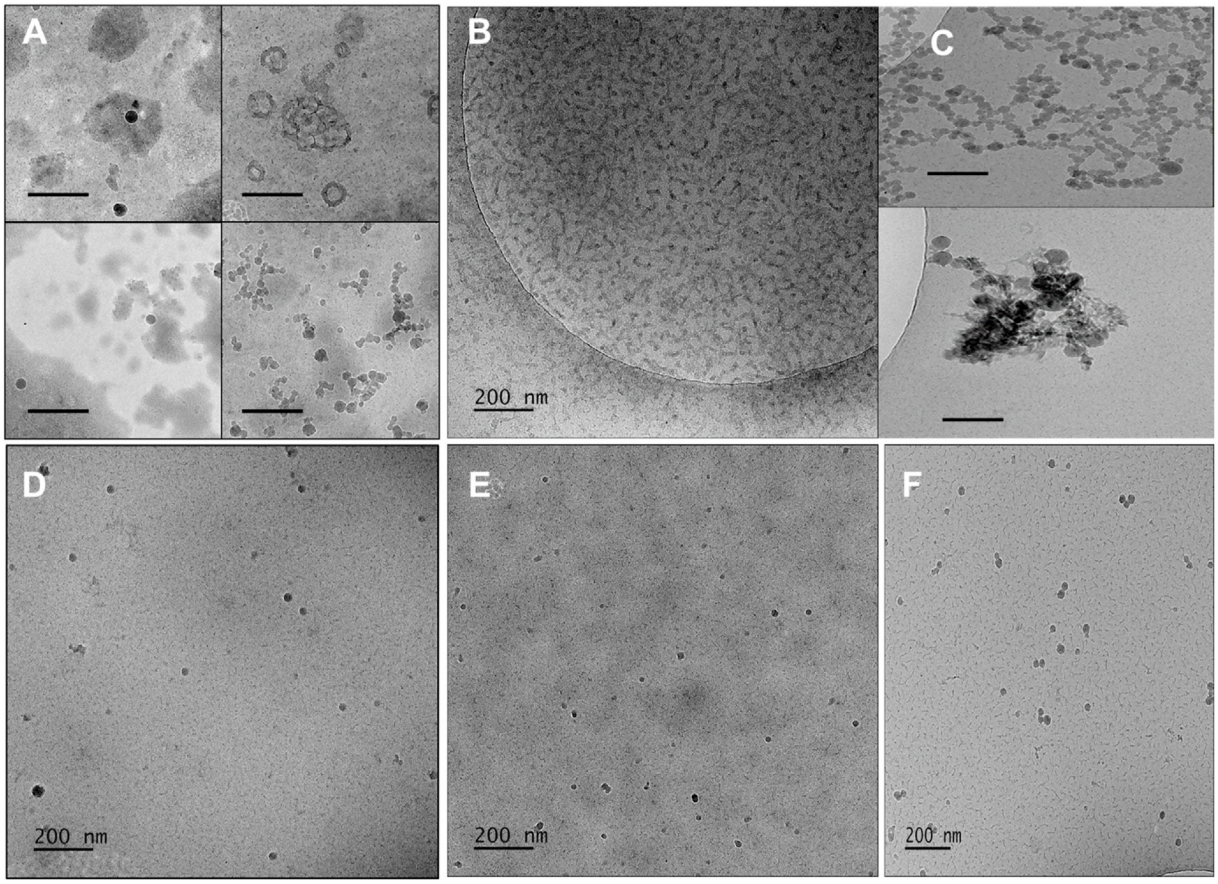

Fig. 7. Cryo-transmission electron microscopy (cryo-TEM) images showing representative assembled structures (samples were subjected to three heating and cooling cycles up to 50 °C: see sub-section 2.7 for detailed sample preparation) for Phe-ELR in water at pH 2.5 (A), pH 4 (B), pH 7 (C), pH 7.4 in PBS (D); and for Ile-ELR in water at pH 2.5 (E), and pH 7 (F). Scale bar 200 nm (the insets have the same resolution as the main image, so the same scale bar is applied to them).

corresponding, amongst others, to the methylene groups vicinal to the carboxylic groups from Glu in both the hydrophilic and hydrophobic blocks, reduced their integration at pH 2.5 by approximately 16 protons, which corresponds to the disappearance of the eight methylene groups vicinal to the carboxylic group in the eight Glu moieties present in the Phe block (Fig. 5).

Thus, these ^{1}H NMR data indicate a much lower mobility and decreased solvation for the F-block and confirm that these hydrophobic residues are aggregated when Glu is in its protonated form, even at low temperatures. Although the above was already anticipated by Urry [35], the NMR analysis in this work corroborates the hydrophobically folded and assembled structure for the F-block irrespective of the presence of the adjacent hydrophilic block, and at any pH. The NMR analysis for this Phe-ELR at higher temperatures shows a marked broadening of the signals and the exclusive presence of the hydrophilic block, with the signals for the F-block remaining absent (Figure S6F). This result is consistent with pre-aggregation of the Phe block and subsequent aggregation of the remaining molecule, with the E-block signals being visible in the spectrum.

Finally, DOSY experiments have been also accomplished (Figure S7). Unfortunately, no significant change in the diffusion coefficient was found in the DOSY spectra of Phe ELR at 5 °C performed at both pHs of 2.5 (Figure S7(a)) and 7 (Figure S7(b)), at which the Phe-ELR is differentially assembled.

Hence, analysis of the NMR spectra allowed us to conclude that the hydrophobic block (F-block) of Phe-ELR is preorganized at low temperatures and even at basic pH.

3.6. Characterization based on thermal techniques

Since thermal techniques are an excellent tool for quantifying the heat capacity of ELR transitions, further evidence for the pre-aggregated state of Phe-ELR was provided by differential scanning calorimetry (DSC). Thus, thermal cycles were applied sequentially in triplicate to quantify if any turbidimetric discrepancies between the first and subsequent cycles were related to energy differences and to verify the reversibility of the transition.

Fig. 6 and Figures S8 to S11 in the Supplementary Information include some representative DSC thermograms obtained under different experimental conditions. The temperature transitions (T_t) and transition enthalpies (ΔH) are summarized in Table 3 as a function of pH for both ELRs.

The behaviour of Ile-ELR is considered first. As can be seen from Fig. 6, while the DSC thermograms are identical at neutral pH, they exhibit clear differences between the first and subsequent cycles at pH 2.5. Differences in T_t and ΔH have been related to concentration [46], presence of salts [48] and mutual influences between blocks related to polarity changes [47].

The higher hydrophobicity of Phe with respect to Ile should result in a higher ΔH and a lower T_t for the former. However, as can be seen from Table 3, the enthalpy values measured for Phe-ELR at pH 2.5 and pH 4 were lower than those for Ile-ELR; furthermore, no transitions were observed for Phe-ELR under neutral pH conditions in either water or PBS.

The results obtained for Phe-ELR point to a less energetic interconversion than expected when compared to Ile-ELR. In other words, the native state of Phe-ELR again seems to be pre-aggregated or "*less*

intrinsically disordered" than Ile-ELR (with "native state" being considered to be that obtained at the lowest temperature used in this study). At low pH an additional process that changes the way in which the polymer transitions thereafter, without significantly affecting the heat capacity of the transition, is suggested for Phe-ELR during self-assembly.

In order to obtain additional information, temperature-modulated differential scanning calorimetry (TMDSC) measurements were carried out. TMDSC is an improved DSC measurement that allows thermally overlapping phenomena with different time dependences to be separated. It has been demonstrated that the endotherm transition of ELRs can be split into a sum of two different contributions: destruction of the ordered hydrophobic hydration structures on heating (endothermic and non-reversing component: slow component), and chain folding and self-assembly once the polymer has lost the hydrophobic hydration (exothermic and reversing component: fast process) [68]. As the phase-separation process is faster than the re-dissolution process [69], an adequate selection of the parameters is required to ensure optimized enthalpy values and, therefore, the splitting of both components. In this work, TMDSC measurements used a temperature program that adds a sinusoidal temperature fluctuation at the appropriate frequency to a constant heating rate, such that the maximum splitting of both components is achieved. The quantitative analysis of the TMDSC thermograms provides the reversing (ΔH_{rev}) and non-reversing ($\Delta H_{non\text{-}rev}$) contributions in the thermal transition (Table S2), a graphical representation of which is shown in Figure S11.

As for Ile-ELR, the magnitude of the exothermic component was about one-third or a quarter lower than that for the endothermic contribution throughout the three cycles (Figure S11), in agreement with results reported for other ELRs [68]. At neutral pH, no noticeable change in the magnitude of both components is observed for the three thermal cycles, whereas at pH 2.5, a significant change is observed between the first cycle and subsequent ones, thus indicating a partial irreversibility. Taking into account both the DSC and TMDSC results for Ile-ELR, a simple conformational rearrangement is suggested for this ELR.

The TMDSC results for Ile-ELR differ markedly from those obtained for Phe-ELR under the conditions in which transitions were detectable (pH 2.5 and pH 4; see Figure S11). Firstly, ΔH_{rev} values show a minimal or residual transition, and these values can be used as a quantitative measurement of the amino-acid hydrophobicity [68]. Specifically, a higher value is found at pH 2.5 than at pH 4 (Table S2). Secondly, despite the obvious differences in the thermogram between the first and subsequent cycles, the energy transitions were very similar between them, with hardly any differences between the contributions analyzed. Thirdly, with regard to the exothermic (providing information about chain folding and assembly) and endothermic contributions (associated with loss of hydrophobic hydration), the former was about sixfold smaller than the latter for pH 2.5 and between 10- and 20-fold smaller for pH 4. As such, we suggest that Phe-ELR undergoes a small conformational reorganization during the first cycle at these pHs, which persists in the following cycles. It may also be proposed a new equilibrium state is reached during this first cycle which allows similar transitions afterwards. Any case, it supports the idea of a pre-aggregated state for this ELR, with Phe-ELR at pH 2.5 being more limited in terms of chain fluctuations than at pH 4.

These energy fluctuations were mirrored in the coacervates that formed after thermal cycling (insets in Fig. 6). At pH 2.5 and pH 4, Phe-ELR formed two different jelly-like assemblies after the heating runs, which were absent at higher pH. A matrix with an unctuous appearance was also obtained for Ile-ELR at the lowest pH, whereas no assemblies were observed under the remaining conditions with this recombinamer.

3.7. Morphological characterization by cryo-TEM

Finally, the morphological characterization of the structures obtained was performed. Fig. 7 shows representative cryo-TEM images for both ELRs, thereby confirming their assembly above T_t.

Phe-ELR is considered first. At pH 2.5, dark spherical aggregates with mean sizes of 31.48 ± 14.88 nm coexist with larger spherical vesicles of lower electron density, which frequently exceed 100 nm. In addition, micellar strings were also observed (Fig. 7A). At pH 4, Phe-ELR self-organizes into worm-like micelles comprising small spheres with a mean size of 15.62 ± 4.56 nm (Fig. 7B).

In the case of Phe-ELR at pH 7 in water, small chains consisting of nanospheres and extensive networks are observed, and in some cases they began to merge, losing their integrity and forming a cluster (Fig. 7C). At pH 7.4 in PBS, Phe-ELR showed uniform and isolated nanoparticles with mean sizes of 21.09 ± 6.04 nm, with no major interactions between them (Fig. 7D).

Some discrepancies are observed between the size obtained by Cryo-TEM and that found by DLS. It should be taken into account the sample preparation required for Cryo-TEM, since grid modification by contact with air may happen at any stage of specimen preparation as D'Imprima et al. [70] have observed. Thus, its impact on protein behavior and structure formation may be significant.

In the case of Ile-ELR, uniform nanoparticle populations with diameters of 19.44 ± 5.56 and 26.12 ± 5.71 nm are observed at pH 2.5 (Fig. 7E) and pH 7 in water (Fig. 7F), respectively. The shaded areas with no definition in Fig. 7E might be interpreted as large aggregates, while in Fig. 7F only occasional pairings are evident. Images of Ile-ELR at pH 7.4 in PBS are not presented in this work since they were previously reported to be highly monodisperse vesicles [23].

In light of the above, the clear differences observed in these morphological assemblies correspond once again to the different behaviour of Phe-ELR and Ile-ELR when their charge distribution is modulated by pH. Although a similar structure and charge distribution might be presumed for Phe- and Ile-ELRs at pH 2.5, their assemblies are far from similar. These differences in the supramolecular assemblies of both polymers observed by cryo-TEM are associated with differences in the secondary structure of these ELRs, which have already been discussed in this paper using different experimental techniques; specifically, the quantitative analysis of the conformations by CD using the BeStSel algorithm suggests that the presence of Phe in the Phe-ELR hydrophobic block impacts on the ELR self-assembly by favouring the formation of secondary structures.

3.8. Overall remarks

The experimental results presented throughout this work have revealed significant differences in the behaviour of Phe-ELR (with respect to the control ELR), such as limited reversibility in thermal cycles, a lower than expected transition enthalpy, and differences in supramolecular assembly.

Our results are in good agreement with recent computational atomistic simulations of short ELR-based peptides, which have shown that the incorporation of bulky aromatic guest residues (phenylalanine in our case) into the elastomeric sequences both tunes the morphology of the assembled ELP conjugate and also gives rise to π-π stacking interactions at low temperatures [71]. Furthermore, Mondal and Haldar [45] highlighted the significant role played by this kind of interaction on their complex out-of-equilibrium phenylalanine-based hydrogel using a combination of experimental techniques.

In this work, we have shown that strong hydrophobic interactions (compatible with π-π stacking interactions) are present even at low temperatures and with high MW ELRs. These interactions provide a high Phe-ELR chain stiffness and this chain only undergoes minor conformational re-arrangements as the temperature increases (for a given pH). The presence of Phe residues enhances the ability of this ELR to coacervate even at 5 °C.

4. Conclusions

In an attempt to clarify the impact of aromatic, hydrophobic amino

acids on the self-assembly and stimuli responsiveness of elastin-like molecular systems, we have produced and characterized two amphiphilic elastin-like diblock co-recombinamers. Thus, the behaviour of our phenylalanine-based ELR has been compared to that of another (control) di-block ELR including Ile. These polymers share structural peculiarities that predict similar functional performances as IDPs, such as low sequence complexity, the same proportion of PG structure-breaking residues, and similar polarity distribution in the different blocks. In the case of the Phe-based hydrophobic segment, the excess of hydrophobicity predicted by Urry is partly compensated by the presence of a glutamic residue, thus meaning that these polymers retain the potential to show transition temperatures in a convenient range.

We have also shown that the presence of Phe residues in the amino-acid sequence gives rise to strong hydrophobic interactions (compatible with π-π stacking interactions) that help to stabilize the structure under the experimental conditions considered. A small conformational organization during the first thermal cycle enhances the ability of this ELR to coacervate, even at the lowest temperature assayed and irrespective of the presence of the adjacent hydrophilic block. In addition, this arrangement shows a clear non-reversible component as these Phe-ELRs undergo a kind of denaturalization event that is not seen in other ELRs. In addition to these interactions, noticeable differences in the behaviour of Phe-ELR (with respect to the control ELR), such as partial reversibility in thermal cycles, a lower than expected transition enthalpy, and differences in supramolecular assembly, are observed experimentally. Thus, a pre-aggregated state of the Phe-ELR under any condition of pH and temperature determines both the initial and final assembly of this ELR in aqueous solution as the temperature increases. This pre-organization is key to the formation of Phe-core nanoparticles or a solid jelly-like material, depending on the concentration. Modulation of the number of negative charges on glutamate for a given pH, and the presence of salts, also have an impact on the size of the nanoparticles and the solidity of the jelly-like coacervate.

This study represents a step forward in our understanding of the underlying mechanisms that predetermine the reversibility of the phase transition of IDPs and sequence-structure relationships that modulate the self-assembly behavior of ELRs. This finding may explain why aromatic segments are rarely present in natural IDPs (e.g., elastin).

Credit Author Statement

All authors have contributed in the same way to the realization of this work.

Declaration of competing interest

The authors declare that they have no known competing financial interests or personal relationships that could have appeared to influence the work reported in this paper.

5. Acknowledgements

The authors are grateful for funding from the Spanish Government (MAT2016-78903-R, RTI2018-096320-B-C22), Junta de Castilla y León (VA317P18), Interreg V España Portugal POCTEP (0624_2IQBIO-NEURO_6_E) and Centro en Red de Medicina Regenerativa y Terapia Celular de Castilla y León.

Appendix A. Supplementary data

Supplementary data to this article can be found online at https://doi.org/10.1016/j.mtbio.2022.100400.

Associated content

Supporting Information (PDF): Analysis of ELRs purity (Figure S1). Acid-base titration (Figure S2), Representative DLS curves (Figure S3). Additional CD data (Table S1 and Figure S4). Additional ^{1}H NMR data (Figure S5 and S6). Additional DOSY spectra (Figure S7). Additional DSC data (Table S2 and Figures S8-S11).

References

[1] U.G.K. Wegst, et al., Nat. Mater. 14 (1) (2015) 23.
[2] Y. Mai, A. Eisenberg, Chem. Soc. Rev. 41 (18) (2012) 5969.
[3] D.D. Boehr, et al., Nat. Chem. Biol. 5 (11) (2009) 789.
[4] P.E. Wright, H.J. Dyson, J. Mol. Biol. 293 (2) (1999) 321.
[5] S. Elsharkawy, et al., Nat. Commun. 9 (1) (2018) 2145.
[6] T. Frege, V.N. Uversky, Biochem Biophys Rep 1 (2015) 33.
[7] M. Dzuricky, et al., Biochemistry 57 (17) (2018) 2405.
[8] S. Roberts, et al., FEBS (Fed. Eur. Biochem. Soc.) Lett. 589 (19, Part A) (2015) 2477.
[9] S.R. MacEwan, A. Chilkoti, Biopolymers 94 (1) (2010) 60.
[10] J.C. Rodriguez-Cabello, et al., Nanomedicine 6 (1) (2011) 111.
[11] L.D. Muiznieks, et al., Biochem. Cell. Biol. 88 (2) (2010) 239.
[12] L.D. Muiznieks, F.W. Keeley, ACS Biomater. Sci. Eng. 3 (5) (2017) 661.
[13] J.C. Rodríguez-Cabello, et al., Polymer 50 (22) (2009) 5159.
[14] P. Tompa, Trends Biochem. Sci. 27 (10) (2002) 527.
[15] V.N. Uversky, et al., Proteins: Struct., Funct., Bioinf. 41 (3) (2000) 415.
[16] J. Habchi, et al., Chem. Rev. 114 (13) (2014) 6561.
[17] S.M. Mithieux, A.S. Weiss, Adv. Protein Chem. 70 (2005) 437.
[18] D.W. Urry, J. Phys. Chem. B 101 (51) (1997), 11007.
[19] J. Reguera, et al., J. Am. Chem. Soc. 126 (41) (2004), 13212.
[20] J.A. Mackay, et al., Biomacromolecules 11 (11) (2010) 2873.
[21] D.H.T. Le, A. Sugawara-Narutaki, Molecular Systems Design & Engineering 4 (3) (2019) 545.
[22] L. Quintanilla-Sierra, et al., Materials Today Bio 2 (2019), 100007.
[23] C. García-Arévalo, et al., Mol. Pharm. 10 (2) (2013) 586.
[24] J. Pille, et al., Biomacromolecules 18 (4) (2017) 1302.
[25] G. Le Fer, et al., Org. Biomol. Chem. 15 (47) (2017), 10095.
[26] L. Martín, et al., Biomacromolecules 13 (2) (2012) 293.
[27] S. Aluri, et al., Biomacromolecules 13 (9) (2012) 2645.
[28] A. Fernández-Colino, et al., Biomacromolecules 15 (10) (2014) 3781.
[29] C. González-Obeso, et al., Small 16 (51) (2020), 2005191.
[30] S. Elsharkawy, et al., Nat. Commun. 9 (1) (2018) 2145.
[31] K.E. Inostroza-Brito, et al., Nat. Chem. 7 (11) (2015) 897.
[32] M.C. Huber, et al., Nat. Mater. 14 (1) (2015) 125.
[33] A. Girotti, et al., Macromolecules 37 (9) (2004) 3396.
[34] D.W. Urry, et al., Biopolymers 32 (4) (1992) 373.
[35] D.W. Urry, et al., J. Am. Chem. Soc. 114 (22) (1992) 8716.
[36] L. Adler-Abramovich, et al., Nat. Chem. Biol. 8 (8) (2012) 701.
[37] E. Gazit, Faseb. J. : official publication of the Federation of American Societies for Experimental Biology 16 (1) (2002) 77.
[38] M. Genji, et al., Chem. Pharm. Bull. 65 (7) (2017) 668.
[39] R. Cukalevski, et al., ACS Chem. Neurosci. 3 (12) (2012) 1008.
[40] L. Travaglini, et al., J. Colloid Interface Sci. 554 (2019) 453.
[41] A. Yi, et al., J. Nanobiotechnol. 18 (1) (2020) 15.
[42] A. Prhashanna, et al., Biomacromolecules 20 (3) (2019) 1178.
[43] S. Wen-qi, Q. Li-wei, Separ. Purif. Technol. 182 (2017) 247.
[44] V. Singh, et al., Soft Matter 11 (26) (2015) 5353.
[45] S. Mondal, D. Haldar, New J. Chem. 45 (10) (2021) 4773.
[46] M.H. Misbah, et al., Polymer 81 (2015) 37.
[47] A. Ribeiro, et al., Biophys. J. 97 (1) (2009) 312.
[48] G. Pinedo-Martín, et al., Polymer 55 (21) (2014) 5314.
[49] A. Girotti, et al., J. Mater. Sci. Mater. Med. 15 (4) (2004) 479.
[50] D.W. Urry, et al., Chem. Phys. Lett. 239 (1) (1995) 67.
[51] A. Micsonai, et al., Nucleic Acids Res. 46 (W1) (2018) W315.
[52] A. Micsonai, et al., Proc. Natl. Acad. Sci. U. S. A. 112 (24) (2015) E3095.
[53] M.J. Thrippleton, J. Keeler, Angew. Chem. 42 (33) (2003) 3938.
[54] Michelle D. Pelta, et al., Magn. Reson. Med. 40 (2002) S147.
[55] A. Botana, et al., J. Magn. Reson. 208 (2) (2011) 270.
[56] D.W. Urry, Angew Chem. Int. Ed. Engl. 32 (6) (1993) 819.
[57] D.W. Urry, et al., Biopolymers 32 (9) (1992) 1243.
[58] R. Herrero-Vanrell, et al., J. Contr. Release 102 (1) (2005) 113.
[59] X. Ma, et al., J. Phys. Chem. B 116 (1) (2012) 555.
[60] J. Jiang, et al., J. Nanoparticle Res. 11 (1) (2009) 77.
[61] W. Hassouneh, et al., Macromolecules 48 (12) (2015) 4183.
[62] D.W. Urry, Chem. Phys. Lett. 399 (1) (2004) 177.
[63] Y.S. Velichko, et al., J. Phys. Chem. B 112 (8) (2008) 2326.
[64] V.N. Uversky, Protein Sci. 11 (4) (2002) 739.
[65] S. Banskota, et al., Biomaterials 192 (2019) 475.
[66] K.N. Greenland, et al., J. Phys. Chem. B 122 (10) (2018) 2725.
[67] A. Micsonai, et al., Biophys. J. 114 (3) (2018) 174a.
[68] J.C. Rodrıguez-Cabello, et al., Chem. Phys. Lett. 388 (1) (2004) 127.
[69] J. Reguera, et al., Macromolecules 36 (22) (2003) 8470.
[70] E. D'Imprima, et al., Elife (2019) 8.
[71] P.A. Taylor, et al., Molecular Systems Design & Engineering, 2020.